Chaotic attitude dynamics of a LEO satellite with flexible panels

Vladimir S. Aslanov[1,*]

Samara National Research University, 34, Moscovskoe shosse, Samara 443086, Russia

Abstract

This paper deals with the attitude motion of LEO satellites with deployable side panels designed for passive aerodynamic stabilization in a rarefied atmosphere. The influence of the aerodynamic and gravitational torques on the planar attitude motion near the unstable and stable equilibrium positions is studied. The presence of the unstable equilibrium position and small perturbations such as the oscillations of the flexible panels is the cause of chaos. A critical altitude is found above which the chaos is possible. The equations of planar attitude motion of the satellite with deployed flexible panels are obtained. The chaotic behavior of the system is demonstrated through numerical simulations of the attitude motion of a 3U CubeSat. The results of this paper can be used to analyze the applicability of passive aerodynamic stabilization for LEO satellites.

Keywords: LEO satellites; chaotic attitude dynamics; passive aerodynamic stabilization, flexible side panels.

1. Introduction

Currently, LEO satellites, such as CubeSats, are widely used in space flight missions. As of the beginning of 2020, more than 1000 satellites of this type have been

* Corresponding author

[1] E-mail address: aslanov_vs@mail.ru. Website: http://aslanov.ssau.ru

launched, at least 100 are launched every year [1]. There are many science and technology applications of CubeSats [2], i.e. in Earth observation [3], astronomy [4,5], biology [6], etc. Satellites of this type have many advantages. The most obvious of them are low cost and short development time. Also, CubeSats can operate in constellations, which allows to distribute risks and provides backup and redundancy to the mission. Finally, CubeSats pose no threat to aircraft or ground objects at the end of their life cycle, since they completely disintegrate in the atmosphere during reentry. CubeSats come in different sizes, which are based on the standard unit — a cube with side length 10 cm (1U). The most popular are the 3U CubeSats (30 cm x 10 cm x 10 cm), which make up about half of all LEO satellites launched [1,7].

For most applications, the attitude stabilization of LEO satellites is important. The active stabilization can be provided by reaction wheels [8], magnetorquers [9,10], micropulsed plasma thrusters [11,12]. For low-Earth orbits (LEO) and especially very low-Earth orbits (lower that 450 km), where the influence of the atmosphere is significant, the most simple way is to use the passive aerodynamic stabilization (PAS), provided by the restoring aerodynamic torque. In some cases, the aerodynamic torque generated on the satellite body itself is sufficient to maintain its orientation along the orbital velocity vector [13], but better results can be obtained with the deployable side panels [14–16]. When not in use, the panels lie against the sides of the satellite. After deployment, they stay fixed at some angle to the sides, as shown in **Fig.** 1. The passive stabilization due to the deployable panels can be complemented by using magnetic torque [17,18] or center of mass shifting [19].

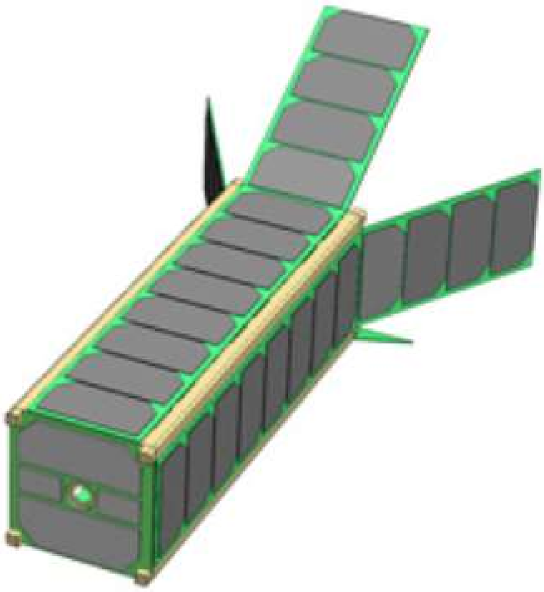

Fig. 1. 3U CubeSat with deployable panels [14].

The stabilizing deployable side panels are inevitably flexible and, while the satellite oscillates under the action of the aerodynamic and gravity gradient torques, they oscillate as well at frequencies different from that of the satellite. When studying the attitude motion of a spacecraft with flexible appendages [20–22], it is convenient to define the unperturbed motion, which in this case is the attitude motion of the spacecraft with appendages assumed to be rigid. Then the motion of the spacecraft with flexible appendages can be considered as the perturbed motion. It is known that if there are unstable equilibrium positions (saddle points) in the unperturbed motion, then even small disturbances can cause chaos in the perturbed motion [23]. In the case of the attitude motion of a satellite with flexible panels the source of these small disturbances is the elastic oscillations of the panels [24,25]. Therefore, instead of stabilizing the attitude motion of the satellite, the panels may, on the contrary, destabilize it due to chaos. It should be mentioned here that the thickness of the chaotic layer depends in a complex way on the system parameters, but near the separatrices, chaos will occur even if the chaotic layer width is small.

The aim of this paper is to show the possibilities and conditions of occurrence of chaos in the attitude motion of a satellite with flexible side panels in a rarefied atmosphere. To demonstrate chaos in the attitude motion, it is enough to take the simplest case of rotation in the orbital plane, since the presence of chaos in a particular case means that it is actually present in the general case. In addition, the planar rotation is the limiting case of the spatial attitude motion. It is in the planar case that the largest amplitudes of the angle of attack are observed, because all the potential energy of attitude motion stored in the satellite is transformed into the kinetic energy of rotation around only one axis.

The paper consists of three main sections. In Section 2 the problem is formulated and the unperturbed motion is analyzed. It is shown that there exists a critical altitude, above which the chaotic attitude motion of the satellite is possible. In Section 3 the equations of motion of the satellite with flexible panels are derived. Section 4 contains two numerical examples for two altitudes illustrating the cases of regular and chaotic attitude motion.

2. Problem statement

In this section, the unperturbed motion of the satellite is analyzed. The below considerations are relevant for any slender body with two equal principal moments of inertia, but to illustrate the idea more clearly, we choose a 3U CubeSat with deployed panels to which we will refer as the example satellite. Its parameters are given in Table 1.

Table 1

Parameters of the example satellite

Parameter	Value
Satellite body length	0.3 m
Satellite body base side length	0.1 m
Satellite body cross-section area	0.01 m^2
Transverse principal moment of inertia of the satellite	0.02 $kg \cdot m^2$
Longitudinal principal moment of inertia of the satellite	0.005 $kg \cdot m^2$
Center of mass longitudinal offset	0.12 m

Panel length	0.2 m
Panel deployment angle	10°
Panel mass per unit length	0.1 kg/m
Panel bending stiffness	$7.1 \cdot 10^{-8}$ N·m^2

We impose the following assumptions.

1. The orbit of the satellite remains circular.
2. All motions take place in the orbital plane.
3. Center of mass of the satellite lies on its longitudinal axis.
4. The aerodynamic characteristics of the satellite do not depend on the oscillations of the panels and Mach number.
5. The aerodynamic damping is negligible.
6. Air density changes with altitude according to the US Standard Atmosphere 1976 [26].

The attitude motion of the satellite depends on two torques: one due to the influence of atmosphere and one due to the gravity gradient. The aerodynamic restoring pitch torque can be written as follows:

$$M_{\mathrm{a}}(\theta,h) = C_{\mathrm{m}}(\theta)q(h)Al, \tag{1}$$

where θ is the pitch angle, h is the altitude, l is the reference length taken equal to the satellite body length, A is the reference area taken equal to the satellite body cross-section area, $q = \frac{\rho V^2}{2}$ is the dynamic pressure, ρ is the air density, $V = \sqrt{\frac{\mu}{R+h}}$ is the orbital velocity, R and μ are the mean radius and gravitational parameter of the Earth, respectively, C_{m} is the aerodynamic restoring pitch torque coefficient. This coefficient was found using the pitch torque data for a 3U CubeSat with the same geometry as the example satellite given in Ref. [15] (Fig. 2, dashed line). The dependence of the aerodynamic torque coefficient on the pitch angle can be approximated by a Fourier sine series (Fig. 2, solid line)

$$C_{\mathrm{m}}(\theta)=\sum_{j=1}^{k} b_j \sin j\theta, \tag{2}$$

where we choose $k=5$, and for b_j we have $b_1=-2.200$, $b_2=0.007$, $b_3=-0.018$, $b_4=0.011$, $b_5=0.103$.

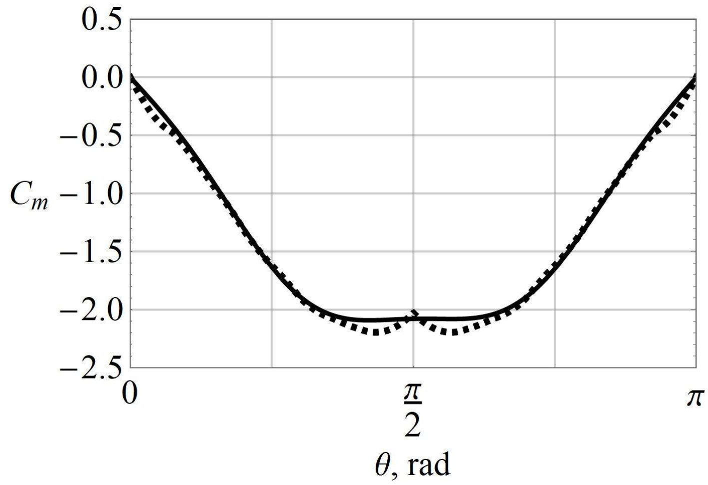

Fig. 2. Aerodynamic pitch torque coefficients of the example satellite (dashed line: data from Ref. [15], solid line: Fourier series approximation)

The gravity gradient torque is defined as

$$M_{\mathrm{g}}(\theta,h)=3\left(J_z-J_x\right)\nu(h)^2\cos\theta\sin\theta, \tag{3}$$

where $\nu=\sqrt{\dfrac{\mu}{\left(R+h\right)^3}}$ is the mean motion, J_z and J_x are transverse and longitudinal moments of inertia of the satellite, respectively.

Since both the aerodynamic and gravitational torques depend only on the pitch angle, it is convenient to analyze the potential energy of the satellite in its unperturbed motion:

$$U_{\mathrm{s}}(\theta,h)=-\int\left(M_{\mathrm{a}}+M_{\mathrm{g}}\right)d\theta=qAl\sum_{j=1}^{k}\frac{b_j}{j}\cos j\theta+\frac{3}{2}\left(J_z-J_x\right)\nu^2\cos^2\theta. \tag{4}$$

Fig. 3 represents the dependency of the potential energy of the example satellite on its altitude and pitch angle. It can be seen that at all altitudes there exist equilibrium positions θ_{s1}, θ_{s2}, θ_{s3}, which are the roots of the equation $M_a + M_g = -\dfrac{\partial U_s}{\partial \theta} = 0$. When $\dfrac{\partial^2 U_s}{\partial \theta^2} > 0$ the equilibrium is stable, when $\dfrac{\partial^2 U_s}{\partial \theta^2} < 0$ it is unstable. At low altitudes, there is only one minimum of the potential energy, at the point $\theta = \theta_{s1} = 0$, corresponding to the stable equilibrium position (**Fig.** 3, bottom right). At high altitudes, the position $\theta = 0$ is unstable (**Fig.** 3, top right), so the PAS along the velocity vector is impossible, but there are two stable equilibrium positions $\theta_{s1} = -\theta_{s2} \neq 0$. The critical altitude h_*, which determines the possibility of the PAS along the orbital velocity vector, can be found from the equation $\dfrac{\partial^2 U_s}{\partial \theta^2} = 0$ with substitution $\theta = 0$. For the example satellite it is about 525 km. The potential energy curve for this altitude is given in **Fig.** 3, middle right.

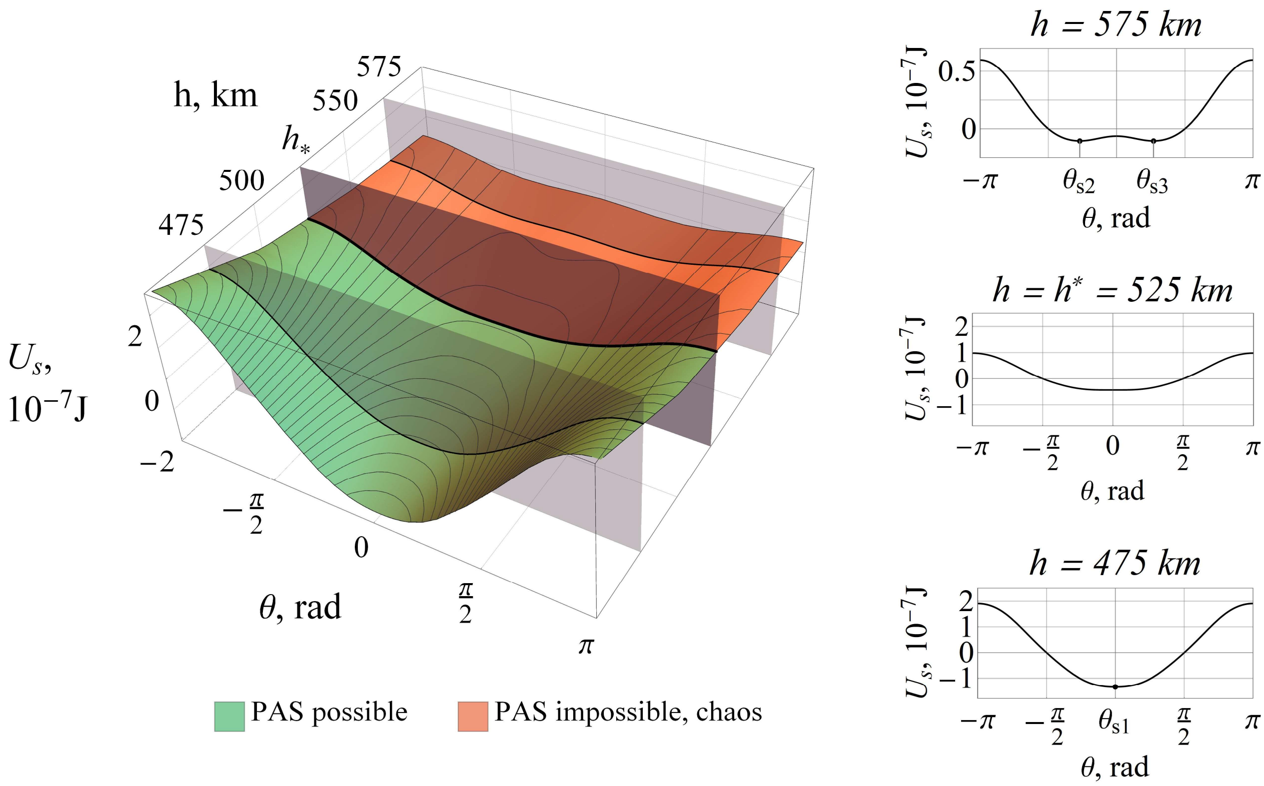

Fig. 3. Potential energy of the example satellite in its unperturbed motion

The evolution of the equilibrium positions with altitude can be represented more clearly by the bifurcation diagram (**Fig.** 4). Below the critical altitude h_*, the aerodynamic torque prevails. As it tends to align the satellite along the orbital velocity vector, the zero pitch angle position is stable. After passing the bifurcation point, the gravity gradient torque, which tends to align the satellite along the local vertical, becomes more significant. This is manifested by the fact that with increasing altitude the stable equilibrium positions approach $\pm\dfrac{\pi}{2}$.

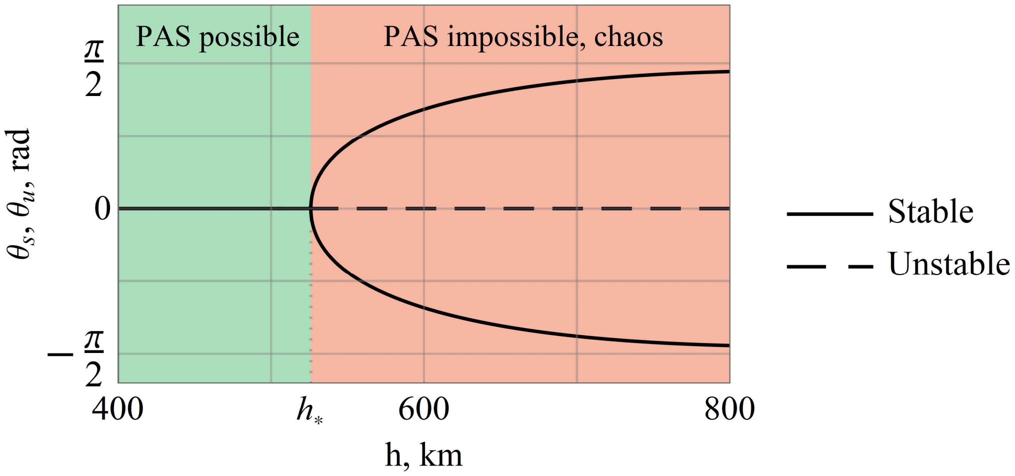

Fig. 4. Bifurcation diagram

3. Equations of motion

In this paper, we use four coordinate frames (**Fig.** 5): the orbital frame OXY, the satellite body-fixed frame Oxy, and two panel-fixed frames $O_1\xi_1\eta_1$ and $O_2\xi_2\eta_2$. The angles δ between the axes Ox and $O_1\xi_1$ and $-\delta$ between the axes Ox and $O_2\xi_2$ can also be regarded as the panel deployment angles. The coordinates of the pivot points of the panels O_1 и O_2 in the Oxy frame are $\left(l_c, \dfrac{a}{2}\right)$ and $\left(l_c, -\dfrac{a}{2}\right)$, respectively, where l_c is the longitudinal offset of the center of mass O, a is the satellite body base side length.

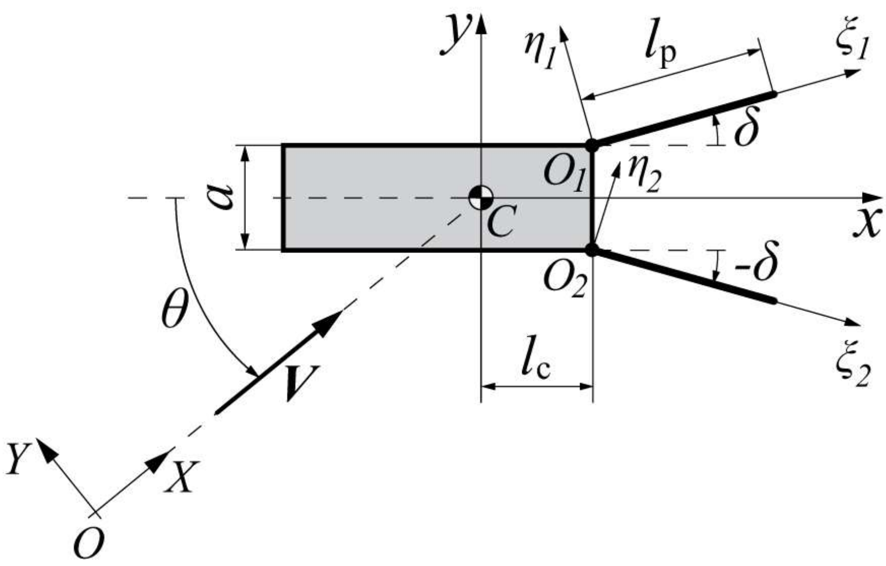

Fig. 5. Coordinate frames

The kinetic energy of the nanosatellite is composed of the kinetic energy of the satellite body T_b and the kinetic energy of the flexible side panels T_p, which are modeled as cantilever beams:

$$T = T_\mathrm{b} + T_\mathrm{p}. \tag{5}$$

The kinetic energy of the attitude motion of the nanosatellite is defined as

$$T_\mathrm{b} = \frac{1}{2} J_z \dot{\theta}^2. \tag{6}$$

The kinetic energy of the flexible side panels is

$$T_\mathrm{p} = \frac{1}{2} \int_0^{l_\mathrm{p}} \left(\boldsymbol{V}_{\mathrm{p}1}^2 + \boldsymbol{V}_{\mathrm{p}2}^2 \right) dm, \tag{7}$$

where l_p is the length of the panel, $\mathbf{V}_{\mathrm{p}i}$ is the velocity of a differential mass element dm of the flexible panel relative to the center of mass, $i = 1, 2$. According to **Fig.** 5, $\mathbf{V}_{\mathrm{p}i}$ can be written as

$$\mathbf{V}_{p1}=\frac{d}{dt}\left[\begin{pmatrix}\cos\theta & -\sin\theta\\ \sin\theta & \cos\theta\end{pmatrix}\cdot\left(\left[l_c,\frac{a}{2}\right]^T+\begin{pmatrix}\cos\delta & -\sin\delta\\ \sin\delta & \cos\delta\end{pmatrix}\cdot[\xi_1,\eta_1]^T\right)\right], \tag{8}$$

$$\mathbf{V}_{p2}=\frac{d}{dt}\left[\begin{pmatrix}\cos\theta & -\sin\theta\\ \sin\theta & \cos\theta\end{pmatrix}\cdot\left(\left[l_c,-\frac{a}{2}\right]^T+\begin{pmatrix}\cos\delta & \sin\delta\\ -\sin\delta & \cos\delta\end{pmatrix}\cdot[\xi_2,\eta_2]^T\right)\right], \tag{9}$$

where ξ_i, η_i are the longitudinal and transverse coordinates of the differential mass element dm of the flexible panel, respectively. The deflection of the flexible panel is defined as

$$\eta_i(\xi_i,t)=\sum_{j=1}^{N}\Phi_j(\xi_i)r_{ij}(t), \quad i=1,2, \tag{10}$$

where $r_{ij}(t)$ are modal coordinates, N is the number of modes considered, and $\Phi_j(\xi_i)$ are the shape functions. The following shape function is an acceptable candidate for a clamped beam [27]:

$$\Phi_j(\xi_i)=B_j\left[\cosh\frac{\omega_j^{1/2}\xi_i}{l_{\mathrm{p}i}}-\cos\frac{\omega_j^{1/2}\xi_i}{l_{\mathrm{p}i}}-d_j\left(\sinh\frac{\omega_j^{1/2}\xi_i}{l_{\mathrm{p}i}}-\sinh\frac{\omega_j^{1/2}\xi_i}{l_{\mathrm{p}i}}\right)\right], \tag{11}$$

where B_j is an unessential constant multiplier taken so that $\Phi_j(l_{\mathrm{p}})=1$,

$$d_j=\frac{\cos\omega_j^{1/2}+\cosh\omega_j^{1/2}}{\sin\omega_j^{1/2}+\sinh\omega_j^{1/2}}, \tag{12}$$

ω_j is a nondimensional natural frequency. For a clamped beam ω_j is defined by the equation [27]

$$\cos\omega_j^{1/2}\cosh\omega_j^{1/2}=-1, \tag{13}$$

where $\omega_1=3.51, \omega_2=22.03, \omega_3=61.70, \ldots$ are the roots of the equation (13).

The potential energy of the satellite equals the sum of the potential energy of the satellite body and the flexible panels, and it can be written as

$$U(\theta,h,\eta_i)=U_{\mathrm{s}}(\theta,h)+U_{\mathrm{p}}(\eta_i), \tag{14}$$

where

$$U_{\mathrm{p}}(\eta_i)=\int_0^{l_{\mathrm{p}}}\left[\sum_{i=1}^{2}EJ\left(\frac{\partial^2\eta_i}{\partial\xi_i^2}\right)^2\right]d\xi_i, \tag{15}$$

EJ is the bending stiffness of the flexible panels, and the functions U_{s} and η_i are defined by the equations (4) and (10), respectively.

We use the Lagrangian formalism to write the motion equations of the system

$$\frac{d}{dt}\frac{\partial L}{\partial\dot{s}_n}-\frac{\partial L}{\partial s_n}=0,\quad n=1,\ldots,3+2N, \tag{16}$$

where $L=T-U$ is the Lagrange function, $s_n=\left(\theta,r_{11},r_{21},\ldots r_{1N},r_{2N}\right)$ are the generalized coordinates. Let us consider only the case when $N=1$, and taking into account (4)–(15), write the Lagrange function in the following simple form:

$$\begin{aligned}L=&\frac{1}{2}a_\theta\dot{\theta}^2+a_{\theta r}\left(\dot{r}_1+\dot{r}_2\right)\dot{\theta}+\frac{1}{2}a_r\left(\dot{r}_1^2+\dot{r}_2^2\right)\\&-c_a\sum_{j=1}^{5}\frac{b_j}{j}\cos j\theta-c_g\cos^2\theta-\frac{1}{2}c_r\left(r_1^2+r_2^2\right),\end{aligned} \tag{17}$$

where

$$a_\theta=J_z+2\mu l_{\mathrm{p}}\left(\frac{1}{3}l_{\mathrm{p}}^2+l_{\mathrm{p}}\left(\frac{a}{2}\sin\delta+l_c\cos\delta\right)+\left(\frac{a}{2}\right)^2+l_c^2\right), \tag{18}$$

$$a_{\theta r}=\mu l_{\mathrm{p}}^2\left(\frac{a}{2}\mathrm{I}_1\sin\delta+l_c\cos\delta+\mathrm{I}_3\right), \tag{19}$$

$$a_r=\mu l_{\mathrm{p}}^2\mathrm{I}_2, \tag{20}$$

$$c_g = \frac{3}{2}\left(J_z - J_x\right)\nu^2, \tag{21}$$

$$c_r = EJl_{\mathrm{p}}^2 \mathrm{I}_4, \tag{22}$$

$$c_a = qAl, \tag{23}$$

μ is a linear mass of the panel, $r_1 = r_{11} / l_{\mathrm{p}}, r_2 = r_{21} / l_{\mathrm{p}}$ are the dimensionless modal coordinates [28],

$$I_1 = \int_0^l \Phi_1(\xi) d\xi, \tag{24}$$

$$I_2 = \int_0^l \Phi_1^2(\xi) d\xi, \tag{25}$$

$$I_3 = \int_0^l \xi \Phi_1(\xi) d\xi, \tag{26}$$

$$I_4 = \int_0^l \left(\Phi_1''(\xi)\right)^2 d\xi, \tag{27}$$

$$\Phi_1(\xi) = \cosh\frac{\omega^{1/2}\xi}{l_{\mathrm{p}}} - \cos\frac{\omega^{1/2}\xi}{l_{\mathrm{p}}} - d_1\left(\sinh\frac{\omega^{1/2}\xi}{l_{\mathrm{p}}} - \sinh\frac{\omega^{1/2}\xi}{l_{\mathrm{p}}}\right), \tag{28}$$

$\omega = 3.51,\ d_1 = 0.81$. Note that exact closed-form results are available in the literature for integrals (24)–(28) for clamped-free beam modes such as the one given in Eq. (28) as well as for other boundary conditions [28].

In numerical simulations, we will also use the total energy of the unperturbed motion which is independent of r_i and $\dot{r}_i$ and has the form

$$E(\theta,\dot{\theta}) = \frac{1}{2}a_\theta\dot{\theta}^2 + c_a\sum_{j=1}^{5}\frac{b_j}{j}\cos j\theta + c_g\cos^2\theta. \tag{29}$$

4. Numerical simulations

The purpose of numerical simulations in this paper is to demonstrate the influence of the altitude of the satellite orbit on the possibility of chaotic pitch motion. We will examine two cases of motion of the example satellite at different altitudes. In Case 1, the altitude of the satellite is 100 km less than the critical altitude h_*, in Case 2, it is 100 km higher than h_*. To make the pitch motions in both cases comparable, the initial conditions $\theta_0, \dot{\theta}_0$ for each case are chosen so that the total energy of the undisturbed motion (29) is the same. In addition, in order to illustrate the deterministic chaos, the mentioned value of the total energy should be close to that of the total energy U_0 on the separatrice for Case 2. The initial conditions of oscillations of the panels $r_{10}, \dot{r}_{10}, r_{20}, \dot{r}_{20}$ are the following: $\dot{r}_{10} = \dot{r}_{20} = 0$, and r_{10}, r_{20} are taken from the uniform distribution on $[-0.05, 0.05]$. Other parameters for the simulations are given in Table 2.

Table 2

Parameters for numerical simulations

Parameter	Value
Altitude for Case 1	475 km
Altitude for Case 2	575 km
Number of simulations for each case	50

4.1. Case 1: altitude lower than critical

Fig. 6 depicts Poincaré sections [29,30] for the case when the example satellite with flexible panels is placed below the critical altitude. The sections are supplemented by a potential energy curve (top left), from which it can be seen that the pitch oscillations of the satellite occur in a potential well, so all possible phase trajectories correspond to the oscillations about a stable equilibrium position θ_{s1}. Let us take one of these trajectories defined by the following initial conditions:

$\theta_0 = 0,\ \dot{\theta}_0 = 0.0034\ \text{s}^{-1},\ r_{10} = -0.0148,\ r_{20} = -0.050,\ \dot{r}_{10} = \dot{r}_{20} = 0.$

Phase diagram of this motion is shown in **Fig.** 7. It can be seen that the pitch angle oscillations have a high-frequency harmonic of small amplitude caused by the flexible panels. **Fig.** 8 illustrates the oscillations of the panels themselves, and it is clear that the panels oscillate in antiphase.

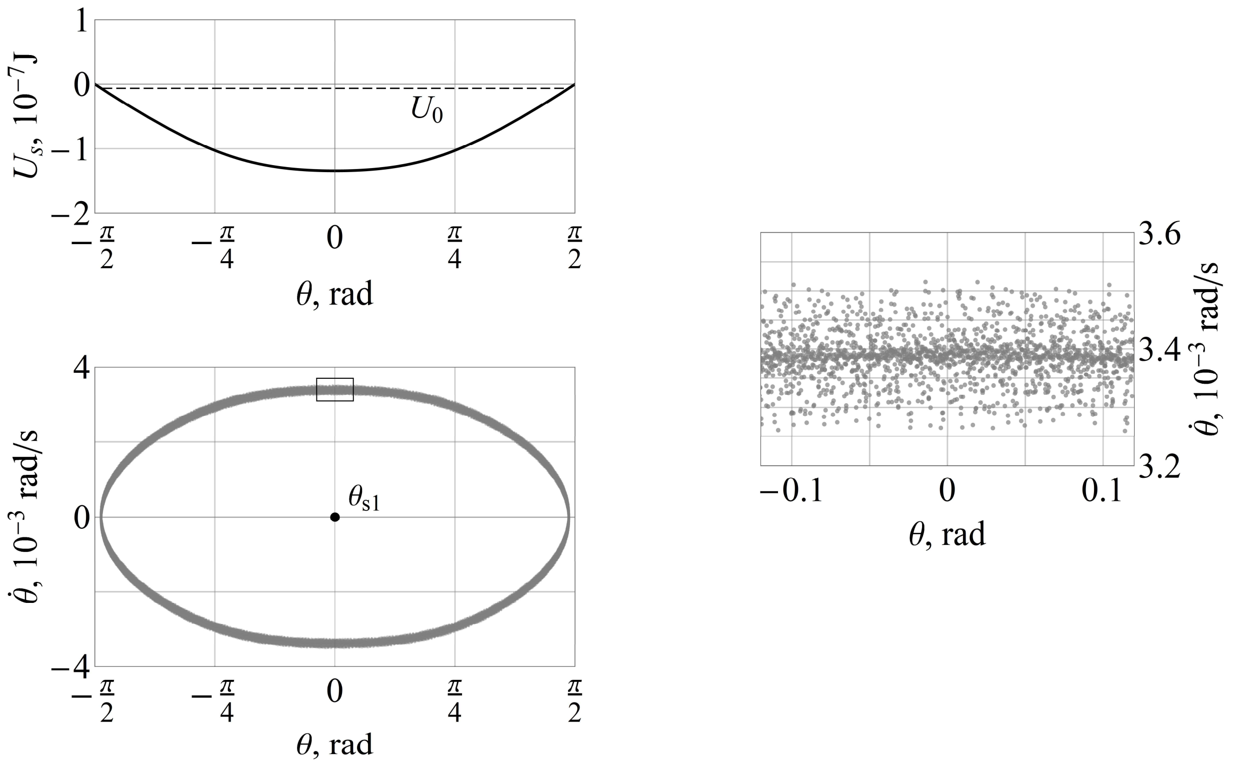

Fig. 6. Poincaré sections for the perturbed pitch motion below the critical altitude

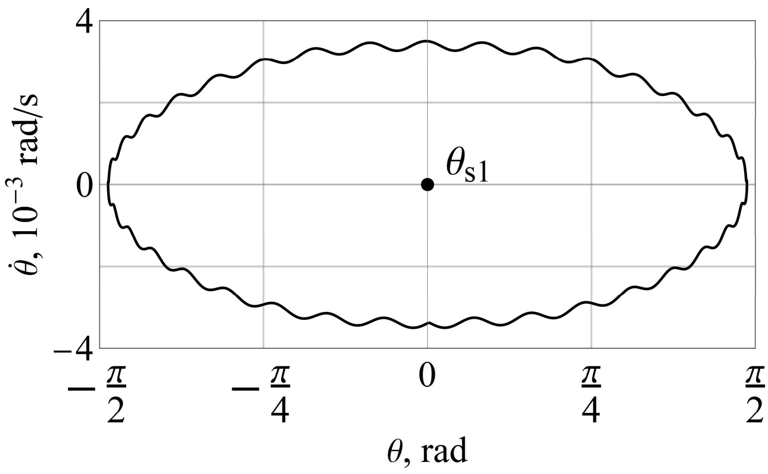

Fig. 7. Phase portrait of a typical regular motion

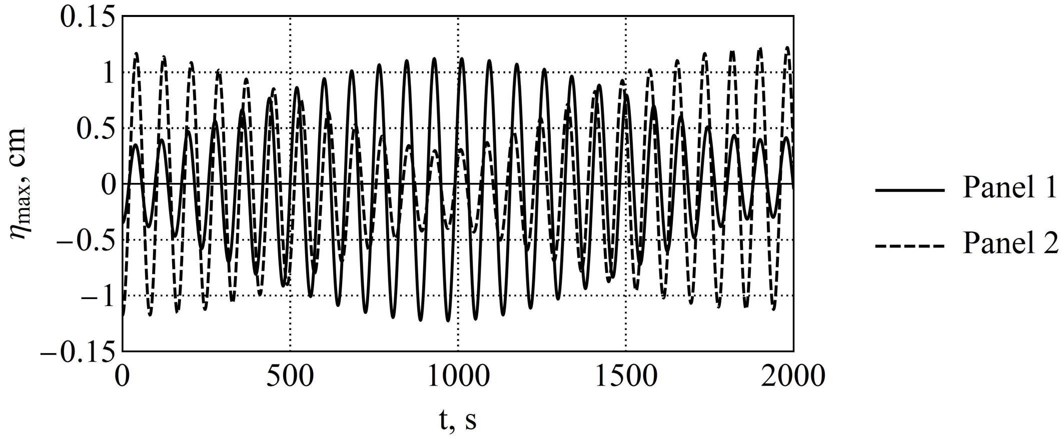

Fig. 8. Time histories of panel tips deflection for a typical regular motion

4.2. Case 2: altitude higher than critical

When the satellite with flexible panels is placed above the critical altitude, the small perturbations in the pitch motion lead to a complication of the phase space and occurrence of a chaotic layer near the unperturbed separatrices. The intersection of stable and unstable manifolds is revealed in the Poincaré plane (**Fig.** 9). Therefore, the occurrence of chaos in the perturbed system is verified. “Построенное сечение Пуанкаре выявляет все исследуемые эффекты и его одного достаточно” As in the previous case, Poincaré sections are supplemented by a potential energy curve, which now has two potential wells and one unstable equilibrium point $\theta = 0$. Due to chaos, phase trajectories may cross the separatrice and pass from one potential well to another. To illustrate this phenomenon, we choose one typical trajectory starting in the vicinity of the unperturbed separatrice defined by the following initial conditions:

$$\theta_0 = 0.038,\ \dot{\theta}_0 = 3.94 \cdot 10^{-5}\ \text{s}^{-1},\ r_{10} = -0.02,\ r_{20} = 0.0014,\ \dot{r}_{10} = \dot{r}_{20} = 0.$$

This trajectory is shown in **Fig.** 10. Initially, the satellite oscillates about the position of stable equilibrium $\theta_{s3} > 0$, and then about another stable point $\theta_{s2} < 0$. Since the initial conditions of the pitch motion correspond to the first quadrant of the phase space inside the separatrices, the fact that the trajectory passes into the region of negative values of pitch angle indicates the intersection of the separatrice, and therefore the presence of chaos. As in the Case 1, the pitch motion has a high-frequency harmonic of small amplitude caused by the elastic oscillations of the panels. Although the deflections of the panel tips are small compared to the panel length (**Fig.** 11), these oscillations are sufficient to cause chaos.

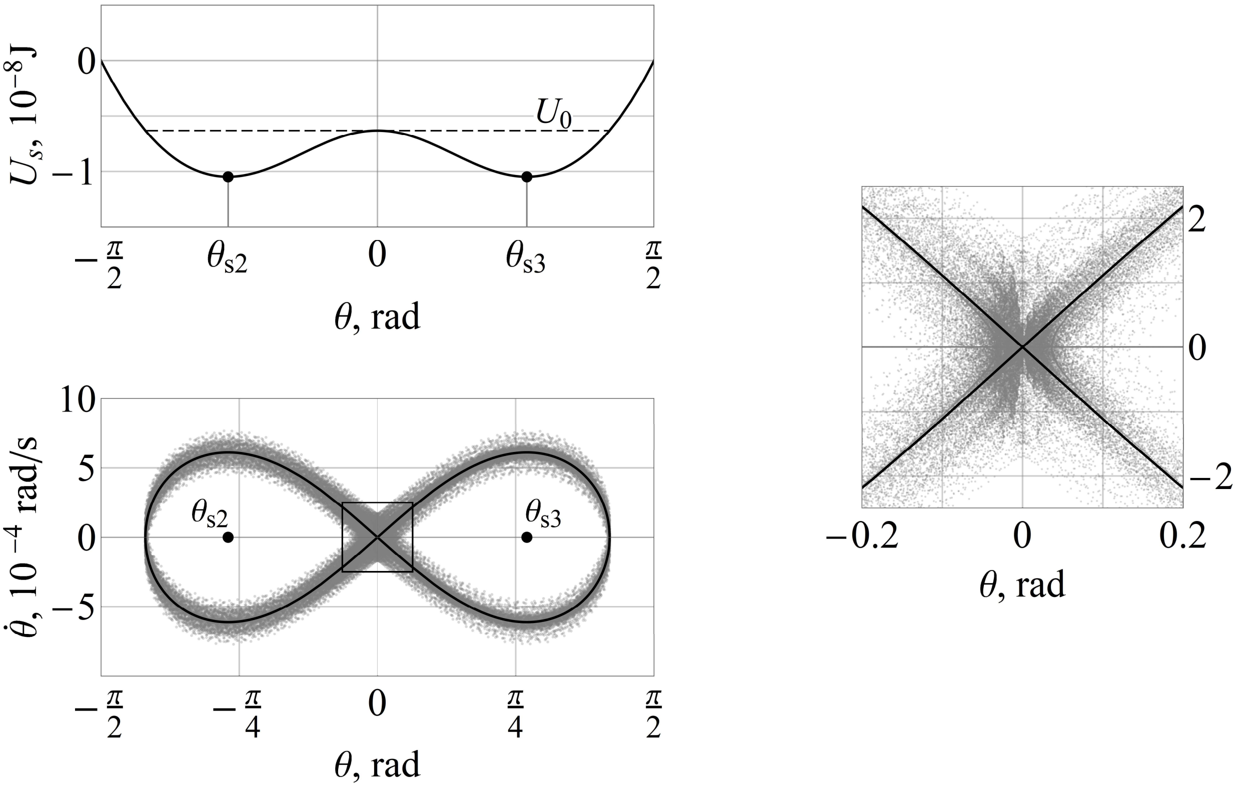

Fig. 9. Poincaré sections for the perturbed pitch motion above the critical altitude

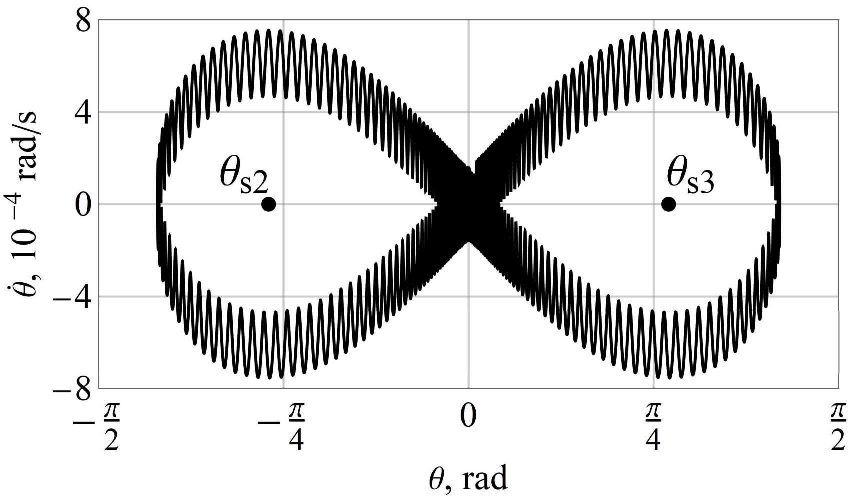

Fig. 10. Phase portrait of a typical chaotic attitude motion

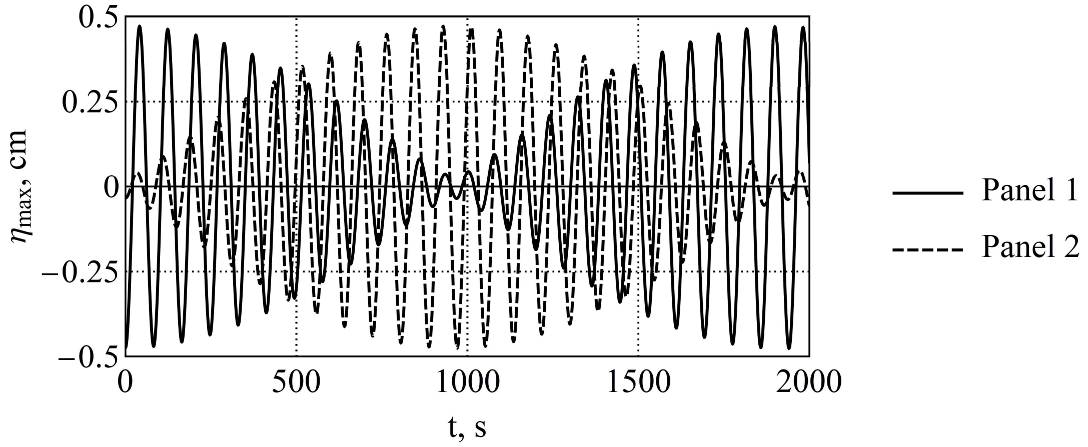

Fig. 11. Time histories of panel tips deflection for a typical chaotic motion

5. Conclusion

The planar attitude motion of LEO satellites with deployable side panels was studied by the example of a 3U CubeSat. The deployable panels are intended for passive aerodynamic stabilization of the satellite along the orbital velocity vector, but they are inevitably flexible, so their oscillations affect the attitude motion of the satellite body. Several steps were taken to investigate the influence of panel oscillations on the stability of the attitude motion of the satellite. First, the satellite with flexible appendages was considered as a rigid body. For a wide range of altitudes, stable and unstable equilibrium positions were found. Next, it was shown that there exists a critical altitude h_* above which the passive aerodynamic stabilization of the satellite is impossible due to chaos. This altitude depends on the mass distribution in the satellite and on its shape. Finally, by numerical simulation, it was demonstrated that for a satellite placed above the critical altitude the deterministic chaos arises in the vicinity of an unstable equilibrium position in the presence of small perturbations such as oscillations of the panels.

This study shows that in order to use the passive aerodynamic stabilization at high altitudes, one has to increase the critical altitude h_* for a given satellite. Future work will focus on the optimization of the mass distribution in the satellite and its shape, including nose section modifications. The general case of chaos in the spatial attitude motion of a satellite in an elliptical orbit is also one of the goals for further studies. In addition, more research is needed to reduce the perturbations. One possible way is to use other types of support for the deployable side panels.

Acknowledgments

This study was supported by the Russian Science Foundation (Project No. 19-19-00085).

References

[1] E. Kulu, Nanosatellite & CubeSat Database, (2020). http://www.nanosats.eu/ (accessed September 28, 2020).

[2] K. Woellert, P. Ehrenfreund, A.J. Ricco, H. Hertzfeld, Cubesats: Cost-effective science and technology platforms for emerging and developing nations, Adv. Sp. Res. 47 (2011) 663–684. https://doi.org/10.1016/j.asr.2010.10.009.

[3] D. Selva, D. Krejci, A survey and assessment of the capabilities of Cubesats for Earth observation, Acta Astronaut. 74 (2012) 50–68. https://doi.org/10.1016/j.actaastro.2011.12.014.

[4] N.C. Deschamps, C.C. Grant, D.G. Foisy, R.E. Zee, A.F.J. Moffat, W.W. Weiss, The BRITE space telescope: Using a nanosatellite constellation to measure stellar variability in the most luminous stars, Acta Astronaut. 65 (2009) 643–650.

[5] C. Underwood, S. Pellegrino, V.J. Lappas, C.P. Bridges, J. Baker, Using CubeSat/micro-satellite technology to demonstrate the Autonomous Assembly of a Reconfigurable Space Telescope (AAReST), Acta Astronaut. 114 (2015) 112–122. https://doi.org/10.1016/j.actaastro.2015.04.008.

[6] S. Canova, F. Fiorasi, M. Mognato, M. Grifalconi, E. Reddi, A. Russo, L. Celotti, "Modeled microgravity" affects cell response to ionizing radiation and increases genomic damage, Radiat. Res. 163 (2005) 191–199. https://doi.org/10.1667/RR3304.

[7] T. Villela, C.A. Costa, A.M. Brandão, F.T. Bueno, R. Leonardi, Towards the thousandth CubeSat: A statistical overview, Int. J. Aerosp. Eng. (2019). https://doi.org/10.1155/2019/5063145.

[8] A.M. Oluwatosin, Y. Hamam, K. Djouani, Attitude control of a CubeSat in a Circular Orbit using Reaction Wheels, in: IEEE AFRICON Conf., 2013: pp. 1–8. https://doi.org/10.1109/AFRCON.2013.6757617.

[9] W.H. Steyn, V. Lappas, Cubesat solar sail 3-axis stabilization using panel translation and magnetic torquing, Aerosp. Sci. Technol. 15 (2011) 476–485. https://doi.org/10.1016/j.ast.2010.09.009.

[10] J. Li, M. Post, T. Wright, R. Lee, Design of attitude control systems for CubeSat-class nanosatellite, J. Control Sci. Eng. 2013 (2013). https://doi.org/10.1155/2013/657182.

[11] N.A. Gatsonis, Y. Lu, J. Blandino, M.A. Demetriou, N. Paschalidis, Micropulsed plasma thrusters for attitude control of a low-earth-orbiting cubesat, J. Spacecr. Rockets. 53 (2016) 57–73. https://doi.org/10.2514/1.A33345.

[12] S. Ciaralli, M. Coletti, S.B. Gabriel, Performance and lifetime testing of a pulsed plasma thruster for Cubesat applications, Aerosp. Sci. Technol. 47 (2015) 291–298. https://doi.org/10.1016/j.ast.2015.09.031.

[13] I. V. Belokonov, I.A. Timbai, P.N. Nikolaev, Analysis and Synthesis of Motion of Aerodynamically Stabilized Nanosatellites of the CubeSat Design, Gyroscopy Navig. 9 (2018) 287–300. https://doi.org/10.1134/S2075108718040028.

[14] S. Rawashdeh, D. Jones, D. Erb, A. Karam, J.E. Lumpp, Aerodynamic attitude stabilization for a ram-facing CubeSat, Adv. Astronaut. Sci. 133 (2009) 583–595.

[15] S.A. Rawashdeh, J.E. Lumpp, Aerodynamic Stability for CubeSats at ISS Orbit, J. Small Satell. 2 (2013) 85–104.

[16] S.A. Rawashdeh, Attitude analysis of small satellites using model-based simulation, Int. J. Aerosp. Eng. (2019). https://doi.org/10.1155/2019/3020581.

[17] M.L. Psiaki, Aerodynamics and Active Magnetic Torquing, J. Guid. Control Dyn. 27 (2004).

[18] R. Sutherland, I. Kolmanovsky, A.R. Girard, Attitude Control of a 2U Cubesat

by Magnetic and Air Drag Torques, IEEE Trans. Control Syst. Technol. 27 (2019) 1047–1059. https://doi.org/10.1109/TCST.2018.2791979.

[19] S. Chesi, Q. Gong, M. Romano, Aerodynamic three-axis attitude stabilization of a spacecraft by center-of-mass shifting, J. Guid. Control. Dyn. 40 (2017) 1613–1626. https://doi.org/10.2514/1.G002460.

[20] V.S. Aslanov, V. V. Yudintsev, Behavior of tethered debris with flexible appendages, Acta Astronaut. 104 (2014) 91–98. https://doi.org/10.1016/j.actaastro.2014.07.028.

[21] V.S. Aslanov, V. V. Yudintsev, Dynamics, analytical solutions and choice of parameters for towed space debris with flexible appendages, Adv. Sp. Res. 55 (2015) 660–667. https://doi.org/10.1016/j.asr.2014.10.034.

[22] V.S. Aslanov, Dynamics of a satellite with flexible appendages in the coulomb interaction, J. Guid. Control. Dyn. 41 (2018) 559–566. https://doi.org/10.2514/1.G002832.

[23] P.J. Holmes, J.E. Marsden, Horseshoes and Arnold diffusion for Hamiltonian systems on Lie groups, Indiana Univ. Math. J. 32 (1983) 273–309.

[24] M. Chegini, H. Sadati, Chaos analysis in attitude dynamics of a satellite with two flexible panels, Int. J. Non. Linear. Mech. 103 (2018) 55–67. https://doi.org/10.1016/j.ijnonlinmec.2018.04.009.

[25] B.Z. Yue, Study on the chaotic dynamics in attitude maneuver of liquid-filled flexible spacecraft, AIAA J. 49 (2011) 2090–2099. https://doi.org/10.2514/1.J050144.

[26] US Standard Atmosphere, (1976). https://ntrs.nasa.gov/citations/19770009539 (accessed September 28, 2020).

[27] S.G. Kelly, Fundamentals of Mechanical Vibrations Any text on mechanical vibrations, (2000).

[28] C.B. Sharma, Calculation of integrals involving characteristic beam functions, J. Sound Vib. 56 (1978) 475–480.

[29] S. Wiggins, Introduction to applied nonlinear dynamical systems and chaos, Springer Science & Business Media, 2003.

[30] F.C. Moon, Chaotic and fractal dynamics: introduction for applied scientists and engineers, John Wiley & Sons, 2008.